FEM-based modelling of NSM-FRP bond behaviour

I. A. Sharaky[1], J. A. O. Barros[2], L. Torres[3]

[1]Zagazig University, Zu, B.O. Box 44519, Zagazig, Egypt/U. Girona, Spain, ibrahim.attia@udg.edu
[2] ISISE, University of Minho, Azurém, 4800-058 Guimarães, Portugal, barros@civil.uminho.pt
[3]University of Girona, Campus Montilivi s/n, 17071 Girona, Spain, lluis.torres@udg.edu

Keywords: Numerical analysis; CFRP; GFRP; Epoxy; NSM; Bond tests.

SUMMARY

Bond between Fibre Reinforced Polymer (FRP) Near-Surface Mounted (NSM) reinforcement and concrete is one of the key factors affecting the behaviour of this strengthening methodology. Properties of FRP, adhesive and concrete greatly affect the effectiveness of the NSM technique. Due to the variety of factors involved in the behaviour of FRP NSM strengthening systems, mechanical models able to incorporate the influencing variables acquire major importance for the prediction of the load capacity and the contribution of the different parameters. By predicting the results obtained in experimental direct pullout tests, a finite element model is adopted to assess the influence of relevant parameters on bond behaviour, namely: bar type, bar size, bond length, epoxy properties and concrete strength. The finite element approach considers interface finite elements for modelling the bond between FRP reinforcement and concrete, and a smeared crack model to simulate the crack initiation and propagation in the surrounding concrete.

1. INTRODUCTION

The near surface mounted (NSM) technique has become a popular method for strengthening RC and masonry members, thereby increasing both flexural and shear strength [1]. The bond behaviour can be affected by the geometric and mechanical properties of the FRPs and adhesives, the geometry of the groove and the quality of the surrounding concrete [2, 3]. Bond failure can occur at the FRP-adhesive or adhesive-concrete interfaces, through adhesive or concrete, tensile rupture of FRP or a combination of these failure modes. The bond behaviour is also sensitive to the test setup [4].

The results reported in [5] indicate that for smooth groove surfaces, concrete-epoxy interface failure was the critical failure mechanism in NSM FRP reinforcement. On the other hand, the results reported in [6] showed that the main failure mode for most of the tested specimens was concrete tension failure, the groove size did not have significant effect on the failure load and the environmental conditions (freeze/thaw cycling) decreased the failure load. However, the results reported in [7] indicated that the local bond strength of the NSM joint increases with the groove dimensions or the groove width (at a constant depth). In addition, the failure load of the NSM joints also increases with the modulus of elasticity and the tensile strength of the adhesive.

In a recent paper the modified pullout test setup described in section 2 was used to study the effect of different combinations of FRP bar types, bar sizes and some construction details on the bond of NSM bars in concrete [8]. The obtained results indicated that construction details (i.e. groove width, and groove shape) have little effect on load capacity, which increased with the bar diameter. Some analytical and numerical models have been proposed to simulate the bond behaviour of NSM reinforcements to concrete [9-12], but in general they are applied to CFRP strips and the concrete

fracture is not considered. In the present paper, a FEM model capable of simulating the FRP-concrete interface, as well as the crack initiation and propagation in the surrounding concrete was used to assess the influence of the following parameters in the local bond slip law: geometric and mechanical properties of FRP and adhesives; bond length and concrete strength. This assessment was performed by fitting as much as possible (inverse analysis) the force vs. loaded end slip responses obtained in direct pullout tests. The experimental program is briefly described, the obtained relevant results are presented (the detailed program can be consulted elsewhere [8]), and the significant findings from numerical research are highlighted.

2. SUMMARY OF THE EXPERIMENTAL PROGRAM

### 2.1. Series of tests, materials and test set up

A total of 23 C-shaped specimens, with the dimensions indicated in Figure 1, were prepared and tested using the modified pullout test. The specimens were tested using the configuration of the modified pullout test described in [5]. The groove was executed by making two saw cuts and using manual hammer to complete the groove formation. The grooves were cleaned using compressed air, and the NSM bars were bonded to the concrete using an epoxy paste in the bond length. The loaded ends of the bars were encased by steel tubes to assure proper gripping conditions of the FRP bars to the testing machine.

FRP properties, bar diameter, adhesive type, concrete strength and bond length are the test variables whose influence in the bond behaviour was investigated. The results of the tested specimens are indicated in Tables 1 and 2 for CFRP and GFRP NSM bars, respectively. The identification of the specimens in the first column of these tables is as follows: the first letter indicates bond length, L_b (L= 192mm and T= 240mm); the following two digits indicate the size (in mm) of the groove's edge (all the grooves had square configuration); the following character represents the adhesive type (A, B, C and D); the following number indicates the type of concrete (1= type 1, 2= type 2); the following two characters represent the type of bar (C= carbon, G= glass, 1= type 1, 2= type 2), and the last number represents the specimen's number (1,2, or 3).

The specimens were cast in series of six, using ready mixed concrete. The compressive and tensile strengths were experimentally obtained from tests performed on standard cylinders (150 × 300 mm). The compressive strengths were 23 and 41 MPa while the tensile strengths were 2.0 and 3.0 MPa, for the type 1 and 2, respectively. Two main types of epoxy resins were used to bond the NSM bars to the concrete substrata, and executing some alterations resulted in four different types of adhesive, as explained below. The first type (A), MBRACE ADHESIVE HT (BASF), consisted of primer and epoxy paste. The second type of resin (B) was POLYFIXER EP (ROBERLO). The properties of resin (B) were modified by adding a special additive (Polypropylene glycol diglycidyl ether, Grilonit® F 704) in two different percentages (1.88%, 3.76%) in order to obtain two more resins with different mechanical properties (C, D). The properties obtained from the tests are 5761, 8000, 7163 and 6900 MPa for the elasticity modulus, and 18.85, 22.95, 22.34 and 21.00 MPa for the tensile strength for epoxy A, B, C and D, respectively. Two types of CFRP bars (C1 and C2) with two diameters, 8 and 9 mm, and GFRP bars of 8 and 12 mm diameter, named G1 and G2, respectively, were used. The pullout tests were performed using a servo-hydraulic testing machine with a displacement controlled rate of 0.003 mm/s up to failure. Two displacement transducers (LVDTs) were used, one to measure the loaded end slip, while the other to measure the free end slip (see Figure 1b).

2.2. Experimental results

The results of the tested specimens are presented in Tables 1 and 2, where: f_{fu} is the ultimate tensile strength of FRP bar; E_f is the elasticity modulus, $E_f A_f$ is the axial stiffness of the bar (A_f is the cross sectional area of the bar), F_{max} is the maximum load, and d_{max} is the loaded end slip at F_{max}. The type of failure mode registered is reported in the last column of this table. In the values indicated in Table 1 for the d_{max}, the elastic deformability of the bar up to the loaded end extremity of the bond length was removed from the recordings in the two LVDTs.

| **(a) Specimen details** | **(b) Test setup** |
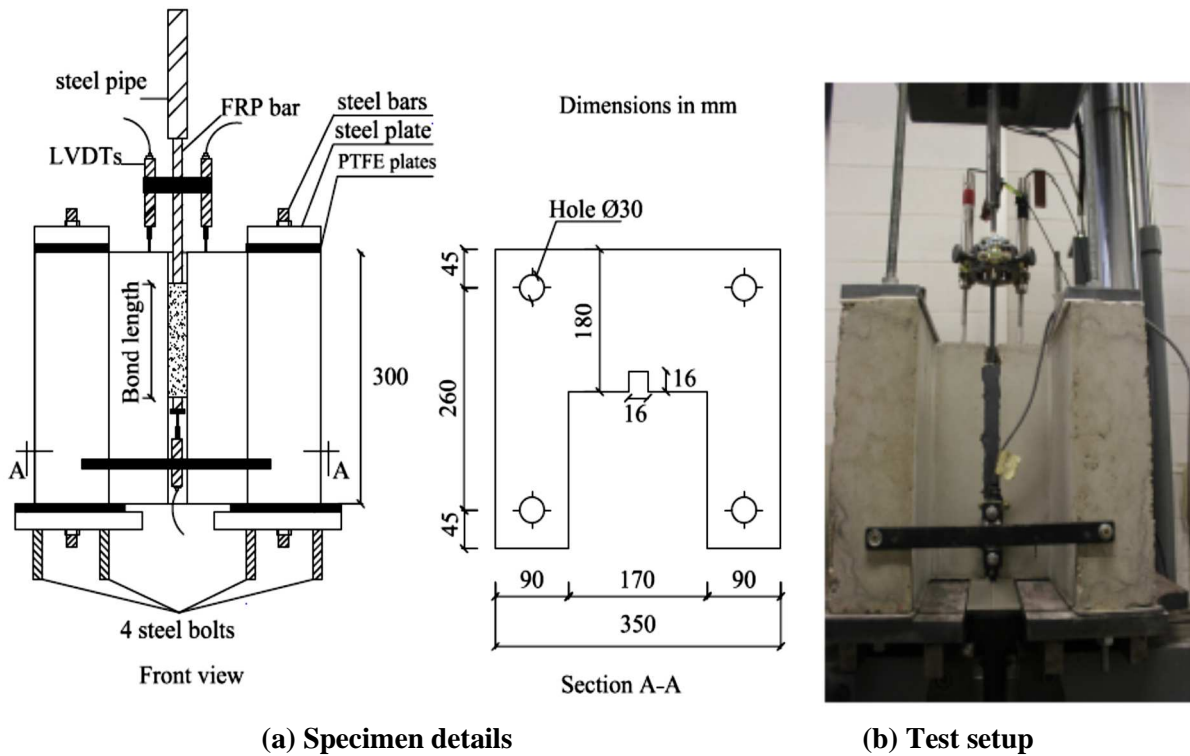
Figure 1: Specimen details and test setup.

The main failure mode of specimens with CFRP bars was bar-epoxy interface failure as shown in Figure 2a. Longitudinal splitting cracks formed on the top surface of epoxy paste in some specimens, especially those bonded with epoxy A. The splitting crack started near the loaded end, and propagated towards the free end of the bonded length up to the occurrence of the failure. At failure concrete surrounding the groove has detached, in specimens reinforced with C2 bars or concrete cracking has occurred in the concrete surrounding the groove.

The main failure mode of specimens reinforced with GFRP bars was epoxy splitting failure followed with detachment of concrete surrounding the groove as shown in Figure 2b. Longitudinal splitting cracks formed on the top surface of epoxy paste in some specimens, especially those bonded with epoxy A (the one with lowest mechanical properties).

This splitting crack started near the loaded end, and during the loading process propagated towards the free end of the bond length up to failure as shown in Figure 2b. On the other hand, in the specimens bonded with epoxy B, C and D some ribs of the bars were scratched followed by bar epoxy interface failure (see Figure 2c) this may be due to the higher properties of adhesive that prevent the formation of longitudinal cracks that allow the bar to slip.

3. NUMERICAL ANALYSIS

3.1. The FEM model

The finite element program FEMIX v4.0 was used to perform an inverse analysis in order to derive the local bond stress-slip law by fitting the pullout force versus loaded end slip registered in the experimental tests [13]. The pullout test configuration shown in Figure 1 was modelled as a plane stress problem. Half part of specimen was considered to reduce the computational time by taking advantages of the structural symmetry conditions (see Figure 3).

3

Table 1: Main experimental data and results from the specimens reinforced with CFRP bars.

| Specimen	f_{fu} (MPa)	E_f (GPa)	E_fA_f (kN)	Epoxy type	f_{cu} (MPa)	F_{max} (kN)	d_{max} (mm)	Failure mode
L16A1C1_1	2350	170	8544	A	23	40.12	0.824	LC, B-E
L16A1C1_2	2350	170	8544	A	23	39.82	0.792	LC, B-E
L16A2C1_1	2350	170	8544	A	41	42.02	0.662	B-E
L15A1C2_1	2010	134	8524	A	23	44.91	0.627	LC, CC, B-E
L15A1C2_2	2010	134	8524	A	23	44.65	0.481	LC, B-E
L15A2C2_1	2010	134	8524	A	41	47.00	0.623	LC ,ES
L16B1C1_1	2350	170	8544	B	23	48.99	0.807	B-E
L16B1C1_2	2350	170	8544	B	23	47.31	0.936	B-E
T16B1C1_1	2350	170	8544	B	23	54.79	1.123	B-E
T16B1C1_2	2350	170	8544	B	23	58.09	1.277	B-E

B-E= bar-epoxy interface failure, ES= epoxy splitting; LC= longitudinal cracking of the epoxy
and CC= concrete tension failure

Table 2: Main experimental data and results from the specimens reinforced with GFRP bars.

Specimen	f_{fu} (MPa)	E_f (GPa)	E_fA_f (kN)	Epoxy type	f_{cu} (MPa)	F_{max} (kN)	d_{max} (mm)	Failure mode
L16A1G1_1	1350	64	3216	A	23	36.23	1.604	LC, CC, ES
L16A1G1_1	1350	64	3216	A	23	38.92	1.300	LC, CC, ES
L16B1G1_1	1350	64	3216	B	23	56.33	3.082	CC, BD
L16B1G1_2	1350	64	3216	B	23	44.56	3.061	CC, BF
L16B1G1_3	1350	64	3216	B	23	48.06	2.678	CC, BF
L16C1G1_1	1350	64	3216	C	23	56.34	2.364	CC, BF
L16C1G1_2	1350	64	3216	C	23	45.36	2.466	CC , BF
L16C1G1_3	1350	64	3216	C	23	52.34	2.863	CC, BF
L16D1G1_1	1350	64	3216	D	23	52.10	3.593	CC,BF
L16D1G1_2	1350	64	3216	D	23	57.79	3.650	BF
L18A1G2_1	1350	64	7238	A	23	59.97	1.256	LC, CS, ES
L18A1G2_2	1350	64	7238	A	23	57.53	0.994	LC, CC, ES
L18A2G2_1	1350	64	7238	A	41	58.59	1.1590	LC,ES

B-E= bar epoxy interface failure, ES= epoxy splitting; CS= concrete splitting, BF= bar surface
damage, LC= longitudinal cracking of the epoxy and CC= concrete tension failure

The four-node Lagrangian plane stress elements with a 2x2 Gauss-Legendre integration scheme was used to simulate the concrete block, while cable 2D linear elements with two integration points were used to simulate the FRP bars. The load was applied on one point of FRP bar (Figure 3), and the arc length method [14] was used by imposing a displacement increment of 0.005 mm at loaded end of FRP bar in direction 3. The FRP bars and the thicker parts of concrete specimen (90×350 mm) were modelled as linear elastic materials. The Young's modulus values for FRP bars (64, 134 and 170 GPa) and for concrete (23 and 30 GPa) determined in the experimental tests were used. Poisson ratio of 0.05 and 0.2 for FRP and concrete were adopted.

| (a) L16A1C1_1 | (b) L16A1G1_1 | (c) L16B1G1_1 |
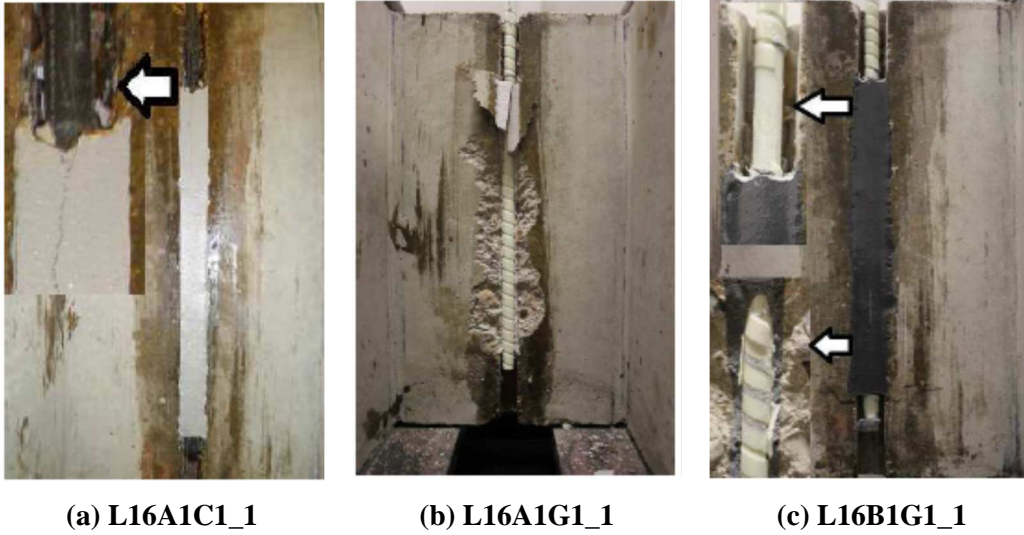
Figure 2: Mode of failure of specimens with NSM CFRP and GFRP bars.

Table 3: Values of the parameters of the concrete constitutive model [14]

Parameters	*Concrete 1*	*Concrete 2*
Poisson's ratio	$v_c = 0.20$	$v_c = 0.20$
Initial Young's modulus	$E_c = 23000$ MPa	$E_c = 38000$ MPa
Compressive strength	$f_c = 23$ MPa	$f_c = 41$ MPa
Strain at peak compression stress	$\varepsilon_{c1} = 2.2 \times 10^{-3}$	$\varepsilon_{c1} = 2.2 \times 10^{-3}$
Tri-linear softening diagram parameters	$f_{ct} = 2.0$ MPa ; $G_f = 0.113$ N/mm $\zeta_1 = 0.4$; $\alpha_1 = 0.8$; $\zeta_1 = 0.6$; $\alpha_1 = 0.2$	$f_{ct} = 3.0$ MPa, $G_f = 0.113$ N/mm $\zeta_1 = 0.4$; $\alpha_1 = 0.8$; $\zeta_1 = 0.6$; $\alpha_1 = 0.2$
Parameter defining the mode I fracture energy available to the new crack yield surface	$P_1 = 2$	$P_1 = 2$
Shear retention factor	*Exponential* ($P_2 = 2$)	*Exponential* ($P_2 = 2$)
Crack band-width	*Square root of the area of the integration point*	*Square root of the area of the integration point*
Threshold angle	$\alpha_{th} = 30°$	$\alpha_{th} = 30°$

For modelling the crack initiation and propagation in the concrete surrounding the FRP systems, the material nonlinear behaviour in the central part of the specimen (with a thickness of 180 mm) was simulated with a multidirectional fixed smeared crack model described elsewhere [14]. The values adopted for the parameters of the constitutive model are indicated in Table 3. The *τ-s* bond law described in Eq. (1) was used to characterize the sliding component of the constitutive law adopted to model the FRP-concrete interface [11], therefore integrating the sliding between FRP-adhesive, adhesive-concrete and the elastic and inelastic deformability of the adhesive. For this purpose, four node line interface finite elements with two-point Lobatto integration rule were used to simulate the bond behaviour between concrete and FRP bar [13]. For the normal stiffness a constant value of 5.0e+05 N/mm² was assumed.

$$\tau(s) = \begin{cases} m_{lin}\, s\,, & s \leq s_{lin} \\ \tau_{max}\left(\frac{s}{s_{max}}\right)^{\alpha}, & s_{lin} < s \leq s_{max} \\ \tau_{max}\left(\frac{s}{s_{max}}\right)^{-\alpha`}, & s > s_{max} \end{cases} \tag{1}$$

In Eq. (1) τ_{max} is the shear bond strength and s_{max} is its corresponding slip, α and α' are parameters defining the shape of the pre and post-peak branches, respectively, and m_{lin} represents the initial stiffness of the bond law, assumed to be linear up to a slip of s_{lin}. The influence of the values of these parameters on the bond behaviour of NSM systems was assessed in a previous work [14].

3.2. Inverse analysis

In the experimental program the loaded end and free end slips were measured directly using LVDTs. In the numerical analysis the τ-s curve was obtained from the results in the sampling point of the interface element closest to the loaded end. The strategy of the inverse analysis was to derive the values of the parameters defining the τ-s bond law that fit with the minimum deviation the pullout force-versus loaded end slip (F-d) up to the failure registered in the experimental tests. The loaded end slip was obtained at $z = 0.0$ (Figure 3b). Since s_{lin} has relatively little influence on the F–d response [15], a value of 0.05 was assumed in all simulations. The values of the parameters of the bond law obtained from inverse analysis for each experimental curve and subsequently averaged for specimen type are listed in Table 3, where $F_{max,num}$ and $F_{max,exp}$ are the maximum pullout forces obtained in the numerical simulations and recorded in the experimental tests, and s_{ult} is the slip at failure (when specimen has failed in the experimental tests).

Figure 4 compares the F-d curves obtained from the inverse analysis to the corresponding ones recorded experimentally. The adopted local τ-s equation seems capable of simulating the global behaviour of all the tested specimens with various NSM bars, epoxy properties, concrete strength and bond length.

(a)   **(b)**
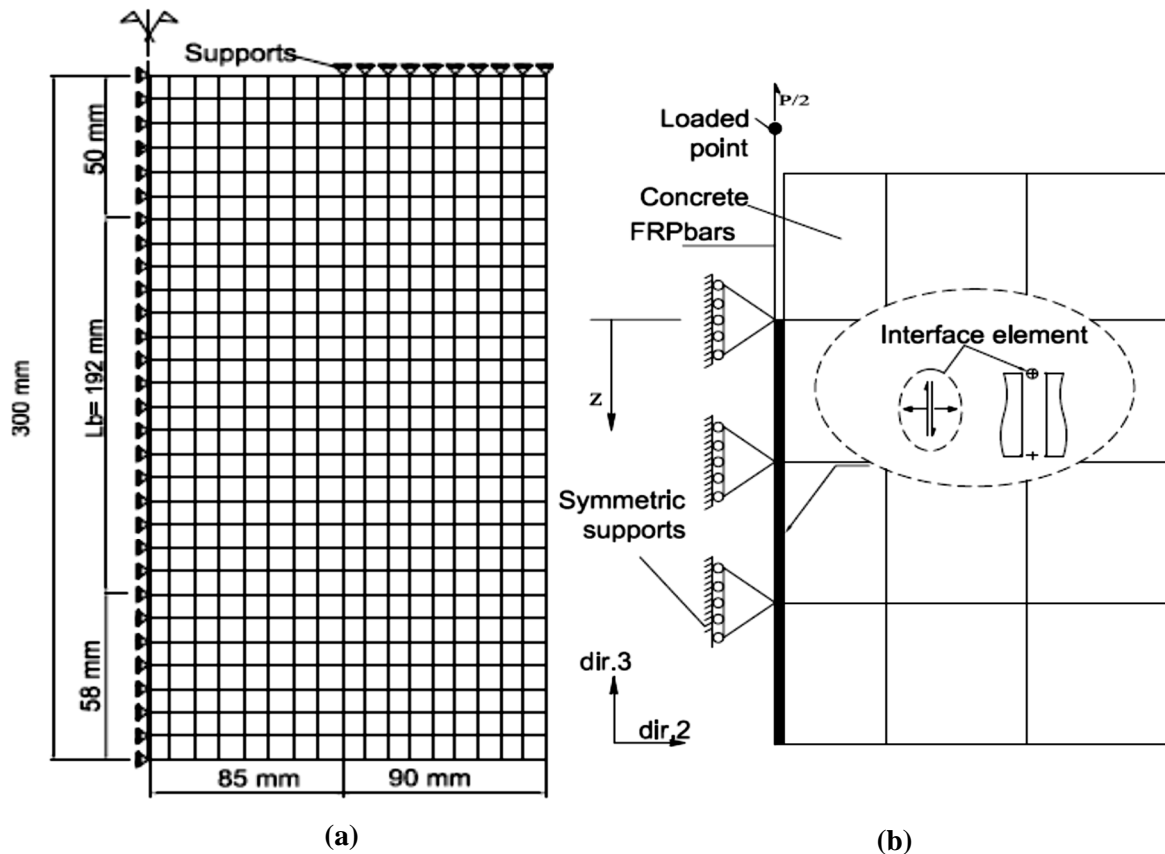
Figure 3: Finite element mesh of half of specimen (a) Complete mesh and (b) Details of the model.

3.3. Influence of the investigated parameters on the local bond law

Figure 5a shows the τ-s curves for specimens with NSM CFRP bars. The two types of CFRP bars, C1 and C2, that have similar axial stiffness, developed similar bond law with slight difference in the value

of τ_{max} (0.25 MPa) and in the post-peak bond stress decay. This difference may be due to the thicker epoxy layer surrounding the NSM in the L16A1C1 specimen (bar diameter of 8 mm and groove dimension of 16 mm edge) than in the L15A1C2 specimen (bar of 9 mm diameter and groove dimension of 15 mm edge). As already demonstrated, during the pullout process micro compressive struts are formed in the cracked adhesive [11, 16]. The force component of these struts normal to the failure crack at the adhesive-FRP interface increases with the decrease of the adhesive layer thickness, which, according to the Mohr-Coulomb principles, justifies the higher post-peak bond strength of the L16A1C1.

The bond law of specimens with NSM C1 bars bonded with epoxy B (the one of highest mechanical properties) presented higher τ_{max} than the τ-s of specimens bonded with epoxy A. The aforementioned reason can also justify this behaviour since as larger is the elasticity modulus of the adhesive as higher is the axial stiffness of the compressive micro-struts of the adhesive, which leads to a stiffer and strong bond connexion. There is also a contribution of the higher tensile strength of epoxy B which in turn delays the formation of micro-cracks. Figure 5a also shows that specimen reinforced with C1 bars bonded with epoxy B developed similar bond law for the two bond lengths, 192 and 240 mm. The main difference is attributed to the slight increase in the value of s_{max} (0.175 mm) in the specimen with larger bond length, which can be justified by the larger volume of the adhesive. Figure 6 shows that, as the concrete strength increases the values of α and α' decrease, due to the smaller deformability and higher confinement provided by the concrete surrounding the bond zone. Due to the same reason, by increasing the concrete strength class the s_{max} has tendency to slightly decrease, while in the CFRP specimens τ_{max} tends to increase moderately.

Figure 5b shows the τ-s curve for specimens with NSM GFRP bars when compared to the τ-s curves of the homologous specimens reinforced with CFRP bars, the τ-s of NSM GFRP bars is characterized by higher values of s_{max} and lower values of α and α', while τ_{max} is similar. The more ductile response of the specimens reinforced with GFRP bars can be attributable to the smaller axial stiffness of these bars (the loaded end slip recorded in the LVDTs also includes the deformability of the bars along the bond length) and their non-smooth surface, since the ribs composing the surface of GFRPs might have contributed to initiate and propagate micro-cracks in the adhesive.

Table 3: Parameters of the bond law and numerical results of tested specimens.

Series ID	s_{max} (mm)	τ_{max} MPa)	α (-)	α' (-)	s_{ult} (mm)	$F_{max,num}$ (kN)	$F_{max,exp}$ (kN)
L16A1C1	0.44	8.80	0.50	0.30	1.54	39.43	39.65
L16B1C1	0.48	10.35	0.48	0.25	5.69	46.67	48.15
L15A1C2	0.43	8.55	0.55	0.15	1.71	44.61	44.72
T16B1C1	0.65	9.90	0.50	0.30	5.69	55.22	56.44
L16A2C1	0.40	9.20	0.30	0.20	0.99	41.42	42.02
L15A2C2	0.35	8.70	0.20	0.35	1.26	45.17	47.00
L16A1G1	0.75	7.90	0.33	0.20	3.03	38.10	37.82
L16B1G1	1.48	10.33	0.27	0.17	4.39	50.80	49.70
L16C1G1	1.35	10.70	0.30	0.23	4.47	51.65	51.40
L16D1G1	1.48	10.33	0.27	0.17	5.82	54.86	54.94
L18A1G2	0.60	8.10	0.20	0.20	1.30	57.83	58.75
L18A2G2	0.50	8.10	0.10	0.10	3.10	59.13	58.59

 Confirming the conclusions already pointed out for the specimens reinforced with CFRP bars, Figure 5b evidences that the strength and stiffness of the local bond law (τ_{max} and s_{max}) increases with the properties of the adhesive, while α and α' are not significantly affected. By comparing L16A1G1 and L18A1G2 it seems that the diameter of the bar has an impact only on the pre-peak phase of the local bond law, by increasing the stiffness of the response with the diameter of the bar.
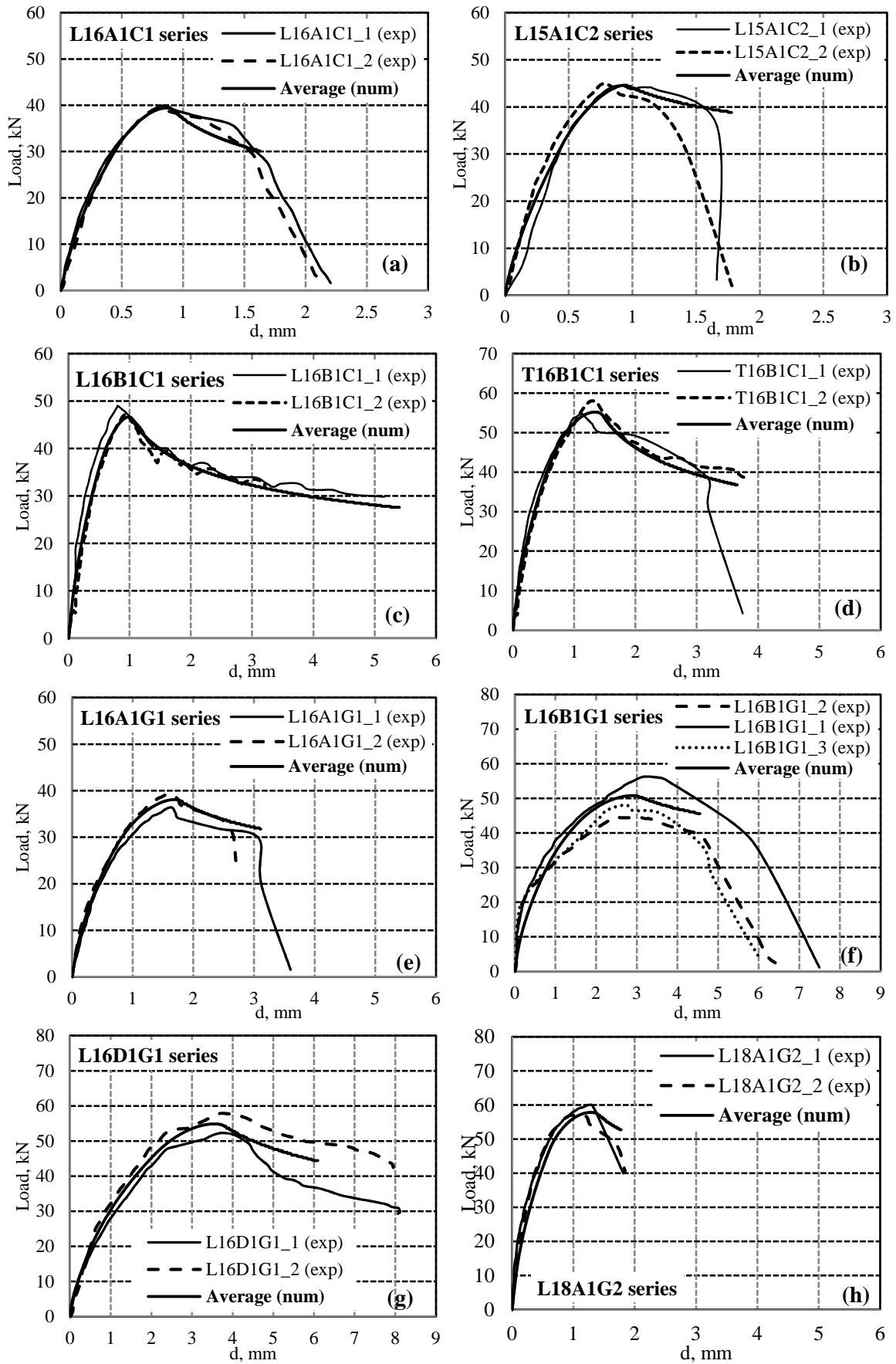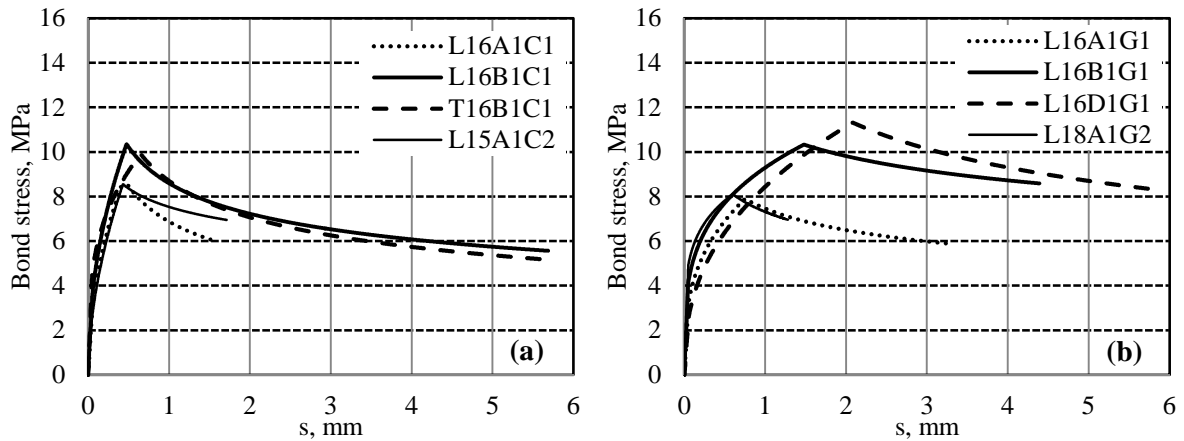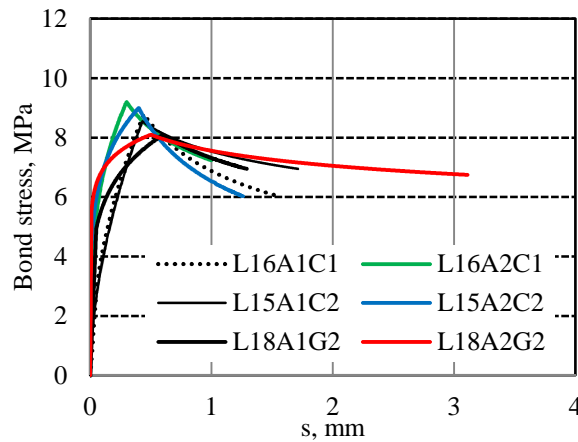
Figure 4: Experimental and numerical *F-d* curves with NSM CFRP and GFRP bars.

Figure 5: Numerical *τ-s* curves (a) Specimens with NSM CFRP bars and (b) Specimens with NSM GFRP bars.

Figure 6: Effect of concrete strength on numerical *τ-s* curves for specimens with NSM FRP

5. CONCLUSIONS

FEM-based modelling of NSM-FRP bond behaviour was used to perform an inverse analysis to derive the local bond stress-slip law from experimental results. The methodology was found to be suitable to analyse and compare the bond behaviour of various types of FRP NSM bars, as well as to assess the influence of relevant parameters. From the analysis performed in this study, the following conclusions can be drawn:

- The obtained local *τ-s* equations were found to be capable of simulating the global behaviour of all the tested specimens with various NSM bars, epoxy properties, concrete strength and bond length.
- The two types of CFRP bars, C1 and C2, that have the same axial stiffness, developed similar bond law with slight difference in the value of τ_{max} and in the post peak stress decay. This difference may be due the thicker epoxy layer surrounding the bar for the case of NSM C1 than that surrounding the NSM C2 bars.
- The larger the elasticity modulus of the adhesive, the higher the axial stiffness of the compressive micro-struts of the adhesive, which leads to a stiffer and strong bond connexion.
- Specimen reinforced with C1 bars bonded with epoxy B developed similar bond law for the two bond lengths, 192 and 240 mm. The main difference is attributed to the slight increase in the value of s_{max} (0.175 mm) in the specimen with larger bond length.
- As the concrete strength increases the values of the parameters defining the shape of the pre and post-peak branches, *α* and *α'*, decrease, due to the smaller deformability and higher confinement provided by the concrete surrounding the bond zone. Due to the same

reason, by increasing the concrete strength s_{max} has tendency to slightly decrease, while in the CFRP specimens τ_{max} tends to increase moderately.

- The local bonds-lip law of NSM GFRP bars is characterized by higher values of s_{max} and lower values of α and α', than those of NSM CFRP bars, while τ_{max} is similar. The more ductile response of the specimens reinforced with GFRP bars can be attributable to the smaller axial stiffness of these bars and to their ribbed surface which might have contributed to initiate and propagate micro-cracks in the adhesive.
- The strength and stiffness of the local bond law for NSM GFRP bars increase with the properties of the adhesive, while α and α' are not significantly affected.

ACKNOWLEDGMENTS

REFERENCES

[1] R. Parretti, and A. Nanni, "Strengthening of RC members using near-surface mounted FRP composites: Design overview", Advances in Structural Engineering,7, 469-483 (2004)

[2] L. De Lorenzis and J. Teng. Near-surface mounted FRP reinforcement: An emerging technique for strengthening structures. Composites Part B: Engineering, 38,119-43 (2007).

[3] A. Palmieri, S. Matthys, J.A.O Barros, I.G. Costa, A. Bilotta, E. Nigro, F. Ceroni, Z. Szambo, G. Balazs, "Bond of NSM FRP strengthened concrete: Round Robin Test Initiative", CICE 2012 6th International Conference on FRP Composites in Civil Engineering, Rome, Italy, 13-15 June 2012.

[4] I.G. Costa and J.A.O. Barros, "Assessment of the bond behavior of NSM FRP materials by pullout tests", First Middle East Conference on Smart Monitoring, Assessment and Rehabilitation of Civil Structures, Dubai, 8-10 February 2011.

[5] L. De Lorenzis, A. Rizzo, A. La Tegola., "A modified pull-out test for bond of near-surface mounted FRP rods in concrete", Composites Part B: Engineering, 33, 589-603 (2002).

[6] S. Soliman, E. El Salakawy, B. Benmokrane., " Bond performance of near-surface mounted FRP bars", Journal of Composites for Construction, 15(1), 103-11 (2011).

[7] D. Galati and L. De Lorenzis., "Effect of construction details on the bond performance of NSM FRP bars in concrete", Advances in Structural Engineering, 12, 683-700 (2009).

[8] I. A. Sharaky, L. Torres, M. Baena, I. Vilanova., "Effect of different material and construction details on the bond behaviour of NSM FRP bars in concrete", Construction and Building Materials, 38, 890-902 (2013).

[9] R. Seracino, N. Jones, M. Ali, M. Page, D. Oehlers.,"Bond strength of near-surface mounted CFRP strip-to-concrete joints", Journal of Composites for Construction, 11, 401-9 (2007).

[10] T. Hassan and S. Rizkalla., "Investigation of bond in concrete structures strengthened with near surface mounted carbon fiber reinforced polymer strips", Journal of Composites for Construction, 7, 248-57 (2003).

[11] S. Cruz and J. Barros., "Modeling of bond between near-surface mounted CFRP laminate strips and concrete", Computers and Structures, 82, 1513-21 (2004).

[12] V. Bianco, J.A.O. Barros, G. Monti, "Bond model of NSM-CFRP in the context of the shear strengthening of RC beams", ASCE Structural Engineering Journal, 135(6), 619-631, June, 2009.

[13] J.M. Sena-Cruz, J.A.O. Barros, A.F. Ribeiro, A.F.M. Azevedo, A.F.F.L. Camões, "Stress-crack opening relationship of enhanced performance concrete", 9th Portuguese Conference on Fracture, ESTSetúbal, Portugal, p. 395-403, 18-20 February (2004).

[14] A. Ventura-Gouveia,"Constitutive models for the material nonlinear analysis of concrete structures including time dependent effects", PhD Thesis, University of Minho (2011).

[15] F. Ceroni, J.A.O. Barros, M. Peece, M. Ianniciello, "Assessment of nonlinear bond laws for nerar-surface-mounted systems in concrete elements", Composites: part B Journal, 45, 666-681, (2013).

[16] J.M. Sena-Cruz, and J.A.O. Barros., "Bond Between Near-Surface Mounted Carbon-Fiber-Reinforced Polymer Laminate Strips and Concrete", ASCE Composites for Construction Journal, 8(6), 519-527, (2004).